Nanoscale

PAPER

View Article Online
View Journal | View Issue

Cite this: *Nanoscale*, 2026, **18**, 12913

Strong and broadband second-order optical nonlinearity through multiple coupled metallic quantum wells

Ching-Fu Chen,†[a] Luke A. Herman †[a] and Zhaowei Liu*[a,b,c]

Received 4th February 2026,
Accepted 7th May 2026

DOI: 10.1039/d6nr00497k

rsc.li/nanoscale

A material system with strong and broadband optical second-order nonlinearity in the near-infrared is theoretically and experimentally demonstrated. Multiple units of TiN-based coupled metallic quantum wells with slightly shifted nonlinear response peaks are uniquely designed and epitaxially grown to form a multilayered stack. By measuring near-infrared to visible second-harmonic generation, second-order susceptibility $\chi^{(2)}$ reaches 740 pm V^{-1} at 900 nm and spreads 200 nm, covering the wavelength range from 800 nm to 1000 nm. Our discoveries open up the possibility to create materials with tailored optical nonlinearity, which can be valuable for building nonlinear optical devices in the fields of bioimaging, ultrafast light source generation, and quantum information technologies.

Introduction

Nonlinear optics harnesses light–matter interactions that emerge when intense light drives the non-perturbative response of materials. Numerous applications exploit the optical second-order nonlinearity of materials, such as optical parametric amplification,[1] optical modulation,[2] on-chip photonic circuits,[3] and quantum information technologies.[4,5] The essential figures of merit of a nonlinear medium are the magnitude and working bandwidth of its optical nonlinearity, described by the second-order susceptibility $\chi^{(2)}$. While optical nonlinearities are weak in naturally existing materials, enhancement mechanisms in novel systems are typically bandwidth-limited. Consequently, there is a critical need to develop materials that simultaneously possess high $\chi^{(2)}$ and support broadband operation.

To solve the issue, some researchers focus on exploring unconventional materials, like GaAs nanowires,[6] $GdCa_4O(BO_3)_3$ (GdCOB) crystals,[7] hybrid plasmonic-dielectric couplers of ZnTe/ZnO single core–shell nanowires integrated with Ag nanoparticles,[8] and epitaxial polydomain barium titanate (BTO) thin films.[9] Others approach the topic by utilizing nanostructures, for example, designing nanoantennas with a bandwidth of several octaves to simultaneously cover both fundamental and harmonic fields,[10] fabricating AlGaInP/Al_2O_3/Ag hybrid plasmonic structures to perform effective excitation in both waveguide and resonant cavity configurations,[11] nanopatterning hyperbolic metamaterials to enhance local field intensity,[12] and combining meta-molecule structures with different geometrical sizes together to construct magnetoelectric coupling which creates artificial nonlinearity.[13] Last but not least, there are several studies using waveguides, for instance, taking advantage of strong self-phase modulation and cross-phase modulation in a dispersion engineered silicon waveguide,[14] constructing broadband phase matching in lithium niobate ($LiNbO_3$) based waveguides.[15–18] Additionally, there is an increasing technological effort to integrate new $\chi^{(2)}$ materials on integrated photonic platforms.[19,20] Even so, these solutions for broadband nonlinear material systems often lack strong nonlinearity or necessitate complex nanolithography.

Recently, asymmetrically coupled quantum wells (cQWs) have become an emerging building block for nonlinear optical devices with ultrahigh optical second-order nonlinearity owing to the engineered doubly resonant inter-sub-band transitions (ISBTs). Record-breaking large $\chi^{(2)}$ is experimentally measured in mid-infrared (MIR) and near-infrared (NIR) ranges using asymmetric semiconductor QWs[21–25] and metallic QWs,[26–28] respectively. The giant nonlinear response has also been demonstrated by coupling resonant ISBTs to plasmonic metasurfaces, which are designed to resonantly enhance the electric field (*E*-field) at fundamental and second-harmonic wavelengths to boost second-harmonic generation (SHG) efficiency.[21,26]

However, one of the concerns of a QW-enabled optical nonlinear platform is the working bandwidth, which is typically limited by the sharp resonance of the ISBTs contributing to the giant optical second-order nonlinearity. To overcome this

[a]*Department of Electrical and Computer Engineering, University of California, San Diego, 9500 Gilman Drive, La Jolla, CA 92093, USA. E-mail: zhaowei@ucsd.edu*
[b]*Materials Science and Engineering Program, University of California, San Diego, 9500 Gilman Drive, La Jolla, CA 92093, USA*
[c]*Center for Memory and Recording Research, University of California, San Diego, 9500 Gilman Drive, La Jolla, CA 92093, USA*
† Contributed equally to this work.

disadvantage, coupled QWs are integrated with metasurfaces or nanocavities, not only to induce large E-field enhancement for higher efficiency, but also to enable a broader working window by designing the plasmonic resonance slightly misaligned to the ISBT resonance.[29] In addition, a recent work demonstrates an electrically tunable broadband nonlinear polaritonic metasurface by combining the Stark tunable nonlinear response of coupled QWs with arrays of nanocavities with different resonant wavelengths.[30] Yet, these studies mainly rely on semiconductor QWs where the working range remains in the MIR.

In this work, we present an ultrathin nonlinear material platform with broad and high $\chi^{(2)}$ in the NIR. This material is made up of multiple units of TiN-based coupled metallic QWs (cMQW), whose peak nonlinear responses differ and span across 800 nm to 1000 nm. Its broadband and strong nonlinear capability is demonstrated by measuring NIR to visible SHG. The result of our study opens the door to a material platform with tailorable nonlinear optical properties, which can be customized to fit specific applications and potentially become the building block for existing nonlinear optical devices.

Theory

Fig. 1 illustrates the design of a material system composed of four cMQW units for broadband optical second-order nonlinearity. Here, an individual cMQW unit consists of two asymmetric TiN QWs with different thicknesses and one ultrathin Al_2O_3 barrier layer in the middle. We apply an electron effective mass of $0.61m_0$, consistent with our previous experimental fits.[24] Note that the adjacent cMQW units share one common TiN QW, which reduces the total thickness of the stack and thus, enables a higher effective nonlinearity. Each cMQW unit supports a doubly resonant transition for the nonlinear process from ω_i to $2\omega_i$ and results in a significant second-order susceptibility $\chi^{(2)}$ peak engineered in the NIR range. By combining these distinct cMQW units to form a multilayered stack, a tailored high $\chi^{(2)}$ profile can be realized to cover a broadband wavelength range from 800 nm to 1000 nm. Therefore, this compact material system becomes a perfect candidate to support efficient broadband nonlinear optics in NIR.

Fig. 2 shows the conduction band diagram and calculated second-order susceptibility $\chi^{(2)}$ of each individual cMQW unit. These theoretical calculations are based on the quantum electrostatic model for ultrathin metallic QWs presented in our previous work.[24] The TiN QWs labeled I–V have thicknesses of 0.8, 1.8, 0.6, 2.2, 1.0 nm, respectively, while the Al_2O_3 barrier layers are 0.5 nm each – thin enough for electron tunneling to occur. Thicknesses of TiN QWs are chosen such that there are three nearly equally spaced electronic sub-bands in each cMQWs unit to support doubly resonant ISBTs, which are critical to produce giant optical nonlinearity. While electron tunneling is necessary for the formation of doubly resonant ISBTs, the ultrathin nature of the inter-cMQW Al_2O_3 barrier layers also introduces weak nearest-neighbor coupling between the cMQW units. Consequently, the discrete energy levels hybridize into broader quasi-minibands,[31] which then relaxes the narrow double-resonance requirement and smooths the spectral response.

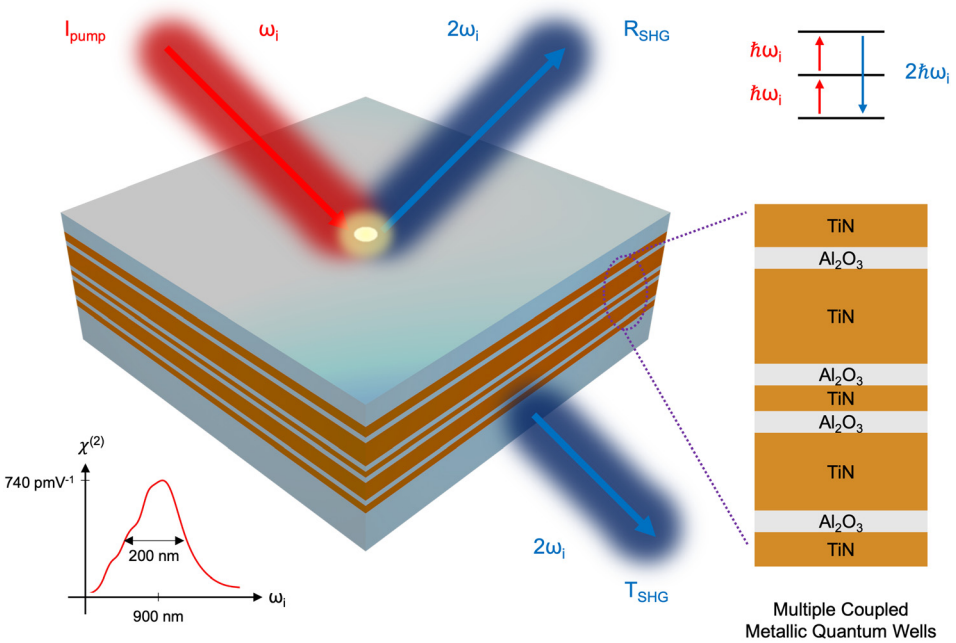

Fig. 1 Schematic of the broadband nonlinear material system consisting of four cMQW units. Each unit supports a doubly resonant ω_i in the NIR range for SHG process from ω_i to $2\omega_i$.

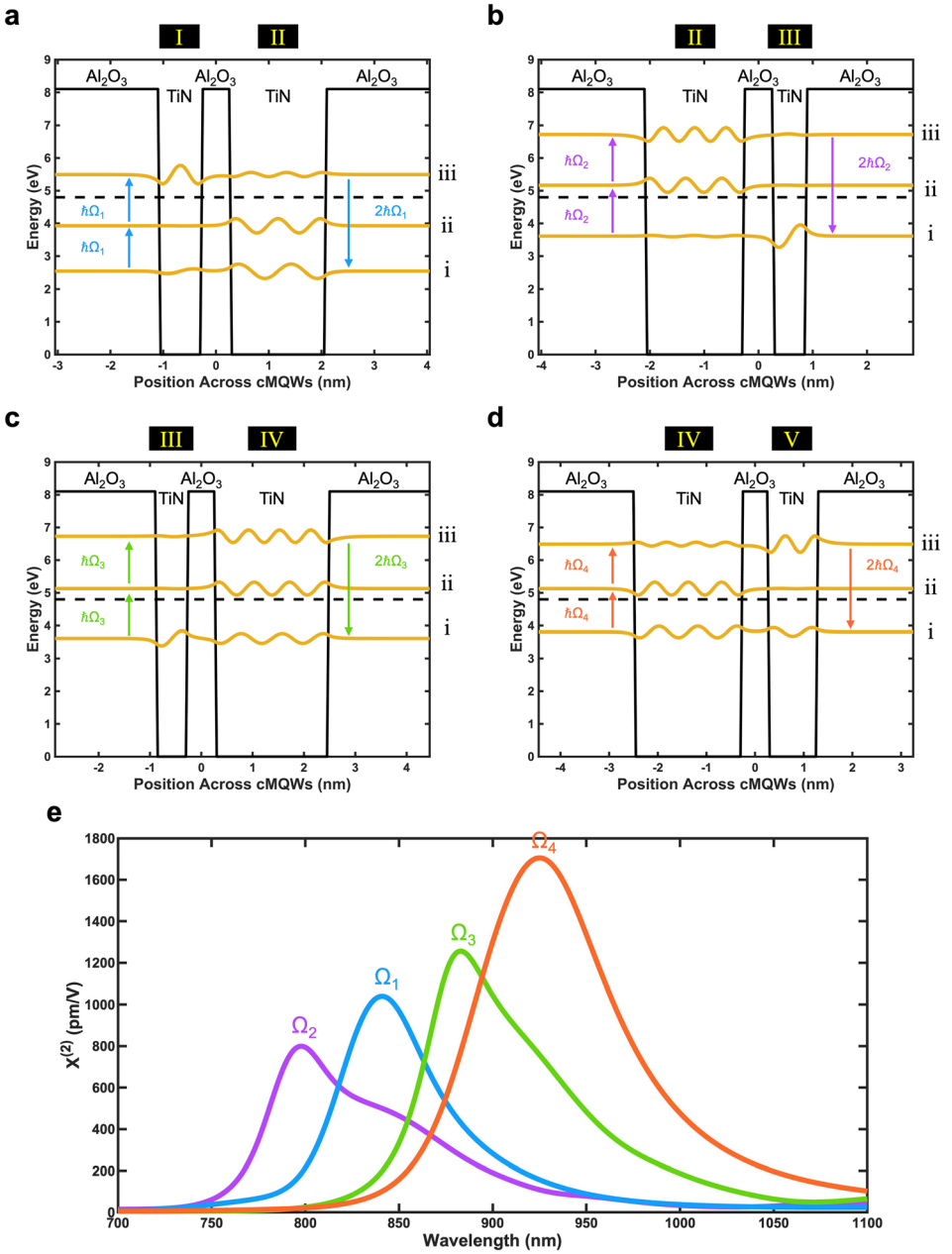

Fig. 2 Theoretical calculation of $\chi^{(2)}$ in cMQWs. (a–d) Conduction band diagrams and the electron wavefunctions near Fermi level (dashed line) of each individual cMQWs unit. In each unit, only the three nearly equally spaced electronic sub-bands that support doubly resonant ISBTs are shown. Thicknesses of TiN QWs labeled I–V are 0.8, 1.8, 0.6, 2.2, 1.0 nm, respectively, while the Al_2O_3 barrier layers are 0.5 nm each. (e) Calculated $\chi^{(2)}$ spectrum of each cMQWs unit.

Fig. 2a depicts the conduction band diagram and the electron wavefunctions associated with the doubly resonant ISBTs in QWs I and II, in which $\chi^{(2)}$ is derived using the following equation:

$$\chi^{(2)}(\omega) = \frac{n_i - n_{ii}}{\hbar^2 \varepsilon_0} \frac{e^3 z_{i,ii} z_{ii,iii} z_{iii,i}}{(\omega - \Omega - i\Gamma_{ii,i})(2\omega - 2\Omega - i\Gamma_{iii,i})} \quad (1)$$

where ω is the incident frequency, Ω is the doubly resonant transition frequency, n_i is the electron density in the i-th sub-band, $\hbar$ is the reduced Planck constant, ε_0 is the vacuum permittivity, and e is the electron charge. Here, $ez_{i,ii}$ and $\Gamma_{ii,i}$ represent the dipole moment and the decay rate associated with certain sub-bands. This leads to a $\chi^{(2)}$ peak centered at 840 nm that reaches ~1040 pm V^{-1}, as shown in blue in Fig. 2e. In a similar way, Fig. 2b–d show the conditions in QWs II–III, III–IV, and IV–V, respectively. This results in three other $\chi^{(2)}$ peaks that are drawn in Fig. 2e: ~800 pm V^{-1} at 800 nm, ~1250 pm V^{-1} at 880 nm, and ~1700 pm V^{-1} at 920 nm. Each color corresponds to the contributing ISBTs in each cMQW unit. While $\chi^{(2)}$ bandwidth of each cMQW unit is narrow, these

units can be further combined together to form a broadband nonlinear material system covering the NIR wavelength range from 800 nm to 1000 nm.

Experimental demonstration

The material system composed of multiple cMQWs units is essentially TiN and Al_2O_3 multilayers. These ultrathin films are epitaxially grown by reactive magnetron sputtering using AJA ATC Orion 8 RF Sputtering System. The substrate chosen is double-side-polished and *c*-plane (0001) oriented sapphire wafers. TiN films are deposited by reactively sputtering a titanium (Ti) target in an argon (Ar) and nitrogen (N_2) mixed chamber, while Al_2O_3 films are deposited by directly sputtering a Al_2O_3 target in an Ar filled chamber. This established technique, developed in our previous works,[26,28] yields metallic TiN QWs and dielectric Al_2O_3 barriers with high-resolution transmission electron microscopy validated atomic-level epitaxy. It is worth noting that no lithography is required to fabricate this material with such broadband nonlinearity since it does not rely on resonance of planar nanostructures.

Fig. 3a shows the optical setup for the broadband nonlinearity measurement, where broadband $\chi^{(2)}$ feature is demonstrated by measuring the SHG signal with illumination at different NIR wavelengths. The Ti:Sapphire femtosecond laser (Spectra Physics – Mai Tai HP) has 100 fs pulse width, 80 MHz repetition rate, and tunable wavelength range from 690 nm to 1040 nm. The dichroic beam splitter allows reflection of light at fundamental wavelength and transmission of SHG signal, while the emission filter further assures that only SHG signal reaches the detector. The detection system is composed of a monochromator and a photon counting detector (Horiba – PPD 850) to capture SHG signal across the spectrum with high sensitivity. The 20× objective lens along with the microscope system (Olympus – IX81) provides illuminating peak intensity of ~5 GW cm^{-2} and collects the output SHG signal at the same time. Fig. 3b presents the four measured second-harmonic emission spectra, centered at 400 nm, 420 nm, 440 nm, and 460 nm, corresponding to four distinct excitations with different fundamental wavelengths. These wavelengths are selected right at the four designed $\chi^{(2)}$ peaks of the multiple cMQWs – namely, 800 nm, 840 nm, 880 nm, and 920 nm. Experimental data are shown in solid black diamonds, while gaussian-fitted curves for each measurement are drawn in different colors.

In addition to these four wavelengths, SHG signals across the spectrum are measured. Thus, effective $\chi^{(2)}$ of the multilayered stack can be further derived, where the multiple

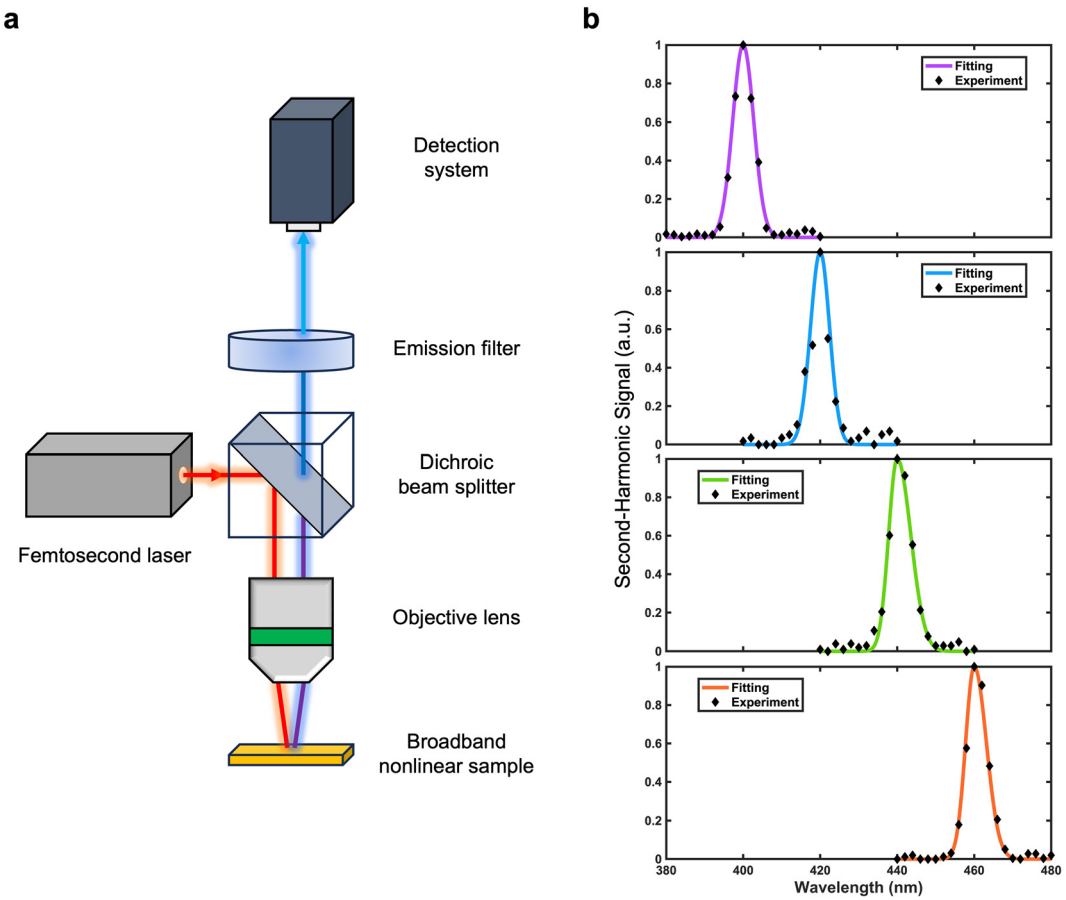

Fig. 3 Optical measurement setup and measured SHG spectra. (a) Optical setup for the broadband $\chi^{(2)}$ characterization. (b) SHG emission spectra under different excitation wavelengths.

cMQWs are treated as a whole material with effective optical properties. The value of $\chi^{(2)}$ is determined according to the following equation:

$$\chi^{(2)}(\omega) = 2\sqrt{\frac{I_{2\omega} n_{2\omega} {n_\omega}^2 c^3 \varepsilon_0}{{I_\omega}^2 \quad 2\omega^2 l^2}} \tag{2}$$

where ω is the incident frequency, $I_{2\omega}$ and I_ω are the peak intensities of output and input signals at second-harmonic and fundamental frequencies, $n_{2\omega}$ and n_ω are the complex refractive indices of the effective medium at second-harmonic and fundamental frequencies, l is the total interaction length of the medium, c and ε_0 represent speed of light in vacuum and vacuum permittivity. The refractive indices at second-harmonic and fundamental wavelengths were determined using effective medium theory from our prior experimental studies on TiN cMQWs.[26] The intensities $I_{2\omega}$ and I_ω are derived from the readings of the photon counting detector for output second-harmonic and the power meter for input fundamental, respectively.

Fig. 4 shows the $\chi^{(2)}$ spectrum obtained from experiment (solid black diamonds) in comparison to the theoretical calculation (red curve). Here, the calculated $\chi^{(2)}$ curve for the multiple cMQWs as a whole is based on weighting the $\chi^{(2)}$ of each individual cMQW unit by its thickness with the following expression:

$${\chi_{\text{total}}}^{(2)} = \frac{{\chi_1}^{(2)} \times t_1 + {\chi_2}^{(2)} \times t_2 + {\chi_3}^{(2)} \times t_3 + {\chi_4}^{(2)} \times t_4}{t_1 + t_2 + t_3 + t_4} \tag{3}$$

where $\chi_i^{(2)}$ is the second-order susceptibility of the i-th set of cMQW unit as shown in Fig. 2e, and t_i is the thickness of that cMQW unit.

The experimental results match well with the theoretical model, where a peak value of $\chi^{(2)}$ reaches ~740 pm V^{-1} at 900 nm along with its full width at half maximum (FWHM) extending nearly 200 nm. The slight discrepancy between experimental and theoretical calculations may be attributed to inter-unit coupling caused by the ultrathin Al_2O_3 barriers, which would broaden the effective nonlinearity further. It is worth noting that the FWHM of $\chi^{(2)}$ is typically less than 100 nm in a single cMQW unit. Therefore, this material system consisting of multiple cMQWs is proven to possess large optical nonlinearity covering a broad working bandwidth in the NIR regime.

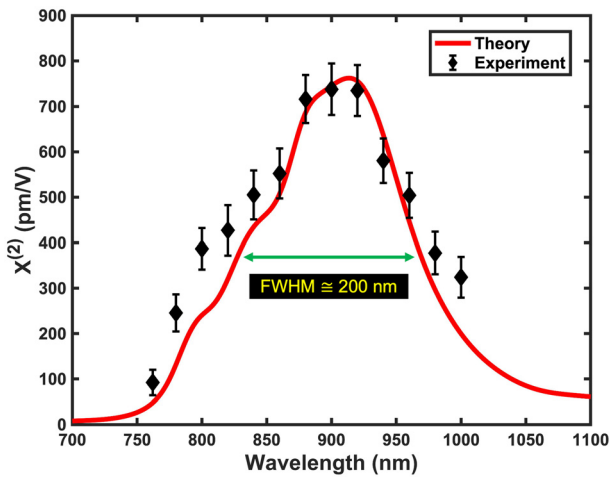

Fig. 4 Measured $\chi^{(2)}$ spectrum in comparison with theoretical calculation.

Discussion

Table 1 presents a comprehensive comparison of the second-order nonlinearity performance of this work with other material systems. When this work of multiple cMQWs units is compared with our previous work of a single cMQW unit, the peak $\chi^{(2)}$ value reduces by 50%, but the relative bandwidth $\Delta\lambda/\lambda_0$ broadens by 340%. The broader bandwidth is obtained at the expense of a lower peak efficiency due to volumetric dilution of the microscopic $\chi^{(2)}$. Both types of cMQW systems can be useful depending on the requirement for specific applications. Common nonlinear crystals such as BBO and $LiNbO_3$ exhibit broad operation bandwidths, yet their peak nonlinearities are only 0.6% and 9.5% of multiple cMQWs. While other material systems from the cited references usually fall short of nonlinear strength, the multiple $In_{0.53}Ga_{0.47}As$-based semiconductor QWs feature extremely high peak $\chi^{(2)}$ value. However, the working wavelength is in the MIR regime. Clearly, the achievement in this work sets a record for large and broad second-order nonlinearity in the NIR range. It is worth mentioning that the working bandwidth can be further extended to the telecom wavelength by adding other designs of cMQW units.

While the multiple cMQWs exhibit large and broad $\chi^{(2)}$, practical device implementation must also account for macroscopic conversion efficiency. The absolute power conversion efficiency from the fundamental wave to the second harmonic wave is approximately 1.05×10^{-10}. This efficiency is fundamentally constrained by the large optical losses of TiN at both the fundamental wavelength (free-carrier absorption) and

Table 1 Comparison of second-order nonlinearity performance

Material system	$\chi^{(2)}$ (pm V^{-1})	λ_0 (nm)	$\Delta\lambda/\lambda_0$ (%)
Multiple TiN-based cMQWs[a]	740	900	22.22
Single TiN-based cMQW[24]	1500	920	6.52
BBO[b]	4.4	680–1700	—
$LiNbO_3$[c]	70	370–5000	—
GdCOB[7]	3.04	1640	9.15
ZnTe/ZnO & Ag[8]	200	840	2.38
BTO[9]	25	3300	18.18
Ag antenna[10]	1.9	2330	19.31
Si waveguide[14]	41	2480	8.06
$LiNbO_3$ on insulator waveguide[15]	38	1500	6.67
Multiple $In_{0.53}Ga_{0.47}As$-based QWs[28]	2×10^5	9750	17.44

λ_0: peak central wavelength; $\Delta\lambda/\lambda_0$: relative working bandwidth. [a] This work. [b] Thorlabs. [c] MTI Corp.

second-harmonic wavelength (interband absorption).[32] Overcoming these material limitations, through metasurface design,[33] effective medium engineering, or novel material stacks[34] represents an exciting research direction.

Conclusions

In summary, we have demonstrated a novel material system exhibiting strong and broadband optical second-order nonlinearity in the NIR. The ability to tune the peak nonlinear response at different wavelengths was validated using distinct cMQW units. By stacking these selected cMQW units, we achieved a broad and high $\chi^{(2)}$ profile spanning from 800 nm to 1000 nm that matches well with our theoretical model. The $\chi^{(2)}$ spectrum reaches a peak of 740 pm V^{-1} at 900 nm, with a FWHM that extends to 200 nm. Ultimately, this work provides a versatile toolkit for scientists to engineer optical nonlinearities built to meet the rigorous demands of future photonic devices.

Author contributions

C. C. and Z. L. conceived the idea. C. C. designed and performed the experiments. C. C. and L. H. performed the theoretical modelling and analyzed the data. C. C. and Z. L. wrote the initial draft. C. C., L. H. and Z. L. reviewed and edited the manuscript. Z. L. acquired the funding and supervised the project.

Conflicts of interest

There are no conflicts to declare.

Data availability

Theoretical and experimental data are available at the Open Science Framework repository at https://doi.org/10.17605/OSF.IO/K64VQ.

Acknowledgements

This work is supported by the National Science Foundation, UCSD MRSEC DMR-2011924. This work was performed in part at the San Diego Nanotechnology Infrastructure (SDNI) of University of California, San Diego (UCSD), a member of the National Nanotechnology Coordinated Infrastructure (NNCI), which is supported by the National Science Foundation (Grant ECCS-1542148).

References

1 C. Trovatello, A. Marini and X. Xu, *Nat. Photonics*, 2021, **15**, 6–10.
2 C. Wang, M. Zhang and X. Chen, *Nature*, 2018, **562**, 101–104.
3 T. P. McKenna, H. S. Stokowski and V. Ansari, *Nat. Commun.*, 2022, **13**, 4532.
4 L. Caspani, C. Xiong and B. J. Eggleton, *Light:Sci. Appl.*, 2017, **6**, e17100.
5 Z. Zhang, C. Yuan and S. Shen, *npj Quantum Inf.*, 2021, **7**, 123.
6 H. He, X. Zhang and X. Yan, *Appl. Phys. Lett.*, 2013, **103**, 143110.
7 X. Zhao, Z. Wang and X. Wang, *Opt. Express*, 2022, **30**, 6546–6555.
8 K.-Y. Nie, S. Luo and F.-F. Ren, *Photonics Res.*, 2022, **10**, 2337–2342.
9 J. Zhou, W. Zhang and M. Liu, *Photonics Res.*, 2019, **7**, 1193–1199.
10 H. Aouani, M. Navarro-Cia and M. Rahmani, *Nano Lett.*, 2012, **12**, 4997–5002.
11 Z. Li, B. Corbett and A. Gocalinska, *Light:Sci. Appl.*, 2020, **9**, 180.
12 J. Li, G. Hu and L. Shi, *Nat. Commun.*, 2021, **12**, 6425.
13 C. Wang, Y. Wen and J. Sun, *Opt. Lett.*, 2021, **46**, 2368–2371.
14 N. Singh, M. Raval and A. Ruocco, *Light:Sci. Appl.*, 2020, **9**, 17.
15 L. Cai, A. V. Gorbach and Y. Wang, *Sci. Rep.*, 2018, **8**, 12478.
16 X. Wu, L. Zhang and Z. Hao, *Opt. Lett.*, 2022, **47**, 1574–1577.
17 C. Zhang, X. Tian and H. Liu, *J. Opt. Soc. Am. B*, 2022, **39**, 3304–3310.
18 Y. Tang, T. Ding and C. Lu, *Opt. Lett.*, 2023, **48**, 1108–1111.
19 J. Frigerio, C. Ciano, J. Kuttruff, A. Mancini, A. Ballabio, D. Chrastina, V. Falcone, M. De Seta, L. Baldassarre, J. Allerbeck, D. Brida, L. Zeng, E. Olsson, M. Virgilio and M. Ortolani, *ACS Photonics*, 2021, **8**, 3573–3582.
20 Ö. E. Aşırım and M. Kuzuoglu, *New J. Phys.*, 2022, **24**, 083046.
21 J. Lee, M. Tymchenko, C. Argyropoulos, P.-Y. Chen, F. Lu, F. Demmerle, G. Boehm, M.-C. Amann, A. Alù and M. A. Belkin, *Nature*, 2014, **511**, 65–69.
22 J. Lee, N. Nookala and J. S. Gomez-Diaz, *Adv. Opt. Mater.*, 2016, **4**, 664–670.
23 N. Nookala, J. Xu and O. Wolf, *Appl. Phys. B*, 2018, **124**, 132.
24 A. Mekawy and A. Alù, *Nanophotonics*, 2021, **10**, 667–678.
25 R. Sarma, J. Xu and D. Ceglia, *Nano Lett.*, 2022, **22**, 896–903.
26 H. Qian, S. Li and C.-F. Chen, *Light:Sci. Appl.*, 2019, **8**, 13.
27 S. E. Bopp, H. Qian and S. Li, *Appl. Phys. Lett.*, 2020, **116**, 241105.
28 C.-F. Chen, H. Qian and Z. Liu, *Adv. Opt. Mater.*, 2024, **12**, 2302176.
29 R. Sarma, D. Ceglia and N. Nookala, *ACS Photonics*, 2019, **6**, 1458–1465.
30 J. Yu, S. Park and I. Hwang, *Nanophotonics*, 2024, **13**, 1131–1139.
31 F. Capasso, A. Tredicucci, C. Gmachl, D. L. Sivco, A. L. Hutchinson, A. Y. Cho and G. Scamarcio, *IEEE J. Sel. Top. Quantum Electron.*, 1999, **5**, 792–807.

32 P. Patsalas, N. Kalfagiannis and S. Kassavetis, *Materials*, 2015, **8**, 3128–3154.
33 M. S. Bin-Alam, O. Reshef, Y. Mamchur, M. Z. Alam, G. Carlow, J. Upham, B. T. Sullivan, J.-M. Ménard, M. J. Huttunen, R. W. Boyd and K. Dolgaleva, *Nat. Commun.*, 2021, **12**, 974.
34 R. An, H. Wang, C. Xie, M. Wu, D. Chu, W. Jin, J. Li, S. Pan and Z. Yang, *Small*, 2025, **21**, 2500540.